Ultramicroscopy ∎ (∎∎∎∎) ∎∎∎–∎∎∎

Contents lists available at ScienceDirect

Ultramicroscopy

journal homepage: www.elsevier.com/locate/ultramic

Full length article

Prospects for quantitative and time-resolved double and continuous exposure off-axis electron holography

Vadim Migunov [a,*], Christian Dwyer [a,c], Chris B. Boothroyd [a], Giulio Pozzi [a,b], Rafal E. Dunin-Borkowski [a]

[a] Ernst Ruska-Centre for Microscopy and Spectroscopy with Electrons, Peter Grünberg Institute, Forschungszentrum Jülich, D-52425 Jülich, Germany
[b] Department of Physics and Astronomy, University of Bologna, viale B. Pichat 6/2, Bologna 40127, Italy
[c] Department of Physics, Arizona State University, Tempe, AZ 85287, USA

ARTICLE INFO

Article history:
Received 15 March 2016
Received in revised form
8 August 2016
Accepted 16 August 2016

Keywords:
Transmission electron microscopy
Off-axis electron holography
Double exposure electron holography
Continuous exposure electron holography

ABSTRACT

The technique of double exposure electron holography, which is based on the superposition of two off-axis electron holograms, was originally introduced before the availability of digital image processing to allow differences between electron-optical phases encoded in two electron holograms to be visualised directly without the need for holographic reconstruction. Here, we review the original method and show how it can now be extended to permit quantitative studies of phase shifts that oscillate in time. We begin with a description of the theory of off-axis electron hologram formation for a time-dependent electron wave that results from the excitation of a specimen using an external stimulus with a square, sinusoidal, triangular or other temporal dependence. We refer to the more general method as continuous exposure electron holography, present preliminary experimental measurements and discuss how the technique can be used to image electrostatic potentials and magnetic fields during high frequency switching experiments.

1. Introduction

The double exposure method in off-axis image plane electron holography was introduced by Wahl [1] as an electron-optical analogue of holographic interferometry, which involves the interference of wavefronts that have been reconstructed from two holograms on the same photographic plate [2,3]. Wahl realised that it is convenient to make a separate recording of the interference fringe system without the specimen present [4] because the processing of the object and vacuum holograms on an optical bench (whether of the in-line or Mach-Zehnder type) allowed more versatility in the reconstruction step.

The re-introduction of double exposure electron holography (DEEH) by Matteucci and co-workers [5,6] was prompted by the increasing application of off-axis electron holography to the investigation of long-range electromagnetic fields, which can extend from a specimen to influence the vacuum reference wave [7]. The moiré fringes that are visible when an object hologram and a vacuum reference hologram are superimposed [8] provide a faithful representation of the phase difference between the object wave and the reference wave (see [9] for a review). Similar moiré patterns have been obtained by the interference of three electron waves using a two biprism holographic setup in an electron microscope [10].

The use of charge-coupled device (CCD) cameras now allows the recording of successive off-axis electron holograms in perfect registry and their *a posteriori* analysis (see *e.g.*, [11]). Digital processing of superposed electron holograms to remove the carrier frequency can be used to increase the contrast of the equiphase fringes, while the superposition of two holograms taken with the object in opposite positions with respect to the biprism can be used to visualise electromagnetic fields with two-times phase amplification [12]. However, to date DEEH has only been used to study a small number of time-varying phenomena, such as ballistic emission from biased nanowires [13] and dynamic charge-related effects around biological specimens [14,15].

Temporal resolution in off-axis electron holography has traditionally been determined by the speed of the detection system. Video-rate electron holography was realised in the early 1990s by the Tonomura group and used for the real-time observation of fluxon dynamics [16]. Although modern detector technology is able to improve temporal resolution to the ms or sub-ms level, phase errors (due to the low signal) then start to play a negative role [17]. A temporal resolution in the sub-μs range would permit studies of fast switching phenomena, such as magnetisation dynamics, with the nm spatial resolution that is offered by electron

* Corresponding author.
E-mail address: v.migunov@fz-juelich.de (V. Migunov).

http://dx.doi.org/10.1016/j.ultramic.2016.08.010
0304-3991/

holography. Recently, DEEH was used to study the magnetic field of the writing head of a hard disk drive, showing its potential for high frequency applications [18]. As we describe below, the technique offers further interesting prospects for ultrafast applications through the continuous acquisition of electron holograms of time-oscillating objects.

We begin by reviewing the original form of DEEH. We then extend the method to applications that involve exposing a detector continuously while the phase shift in the specimen changes, for example as a result of the time-dependent response of the specimen to an external electromagnetic stimulus.

This paper is organised in five sections. In Section 2, we introduce DEEH, providing examples and justifying the method that was developed in the past. Section 3 summarises the underlying theory. To the best of our knowledge, this is the first time that the theory of DEEH has been addressed for electron waves in detail, including equations for the phase of the superimposed waves. We consider the noise figure for the method, compare it to that of traditional electron holography and extend the double exposure method to time-dependent object waves in dynamic experiments. We refer to this more general technique as continuous exposure electron holography. In Section 4, we present possible approaches for extending DEEH using digital analysis. We address the effects of absorption inside the specimen and discuss approaches for the amplification and unwrapping of the recorded phase contour maps. In Section 5, we discuss experimental aspects of studying time-varying phase objects, including proposals for high frequency experiments that involve using different pulse shapes to excite specimens. Conclusions and an outlook are provided in the final section.

2. Basis of double exposure electron holography

Although DEEH was originally realised by exposing the same recording medium (*e.g.*, a photographic plate) to two different electron holograms, the continuous exposure of a detector by an electron hologram while an object switches between two states (without going through any intermediate states) is directly analogous. In both cases, moiré fringes are formed at the positions of equiphase contours that represent the phase difference between the two states.

If a detector is exposed continuously, then DEEH can be realised most easily by recording an electron hologram while applying a time-varying stimulus to the specimen that oscillates between two states. If the stimulus takes the form of a square wave (with a period that is much greater than the time constant of the system), then the result is equivalent to a superposition of two holograms corresponding to the two states, *i.e.*, to the original DEEH method. In this manuscript, we use DEEH to refer to the specific case of a square wave stimulus and the more general term continuous exposure electron holography to describe experiments that involve other oscillatory phase changes.

Fig. 1 shows a schematic representation of the experimental setup that we use to demonstrate the application of a square wave excitation (*i.e.*, for a two level system) using two electrically biased metallic needles mounted in a nanopositioning specimen holder supplied by Nanofactory Instruments AB (Göteborg, Sweden). When a bias voltage is applied between the needles in the form of a square wave, the electric field between the needles oscillates between the two states during acquisition of the hologram. The superposition of holograms corresponding to the two states results in the formation of moiré fringes (see Fig. 2). Regions where the two sets of interference fringes are superimposed in antiphase lose contrast when compared to regions where the two fringe systems interfere in phase, resulting in the appearance of coarse

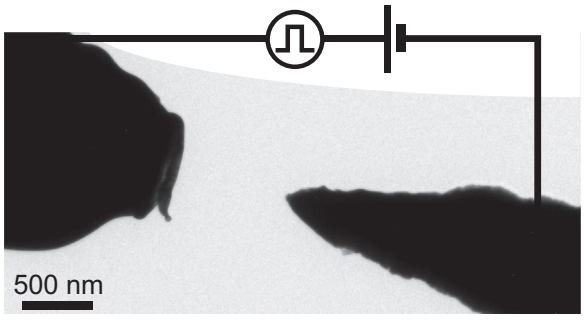

Fig. 1. Bright-field TEM micrograph of the ends of two metallic needles mounted in a Nanofactory specimen holder, overlaid with a schematic circuit diagram showing how a voltage is applied between them in situ in the TEM.

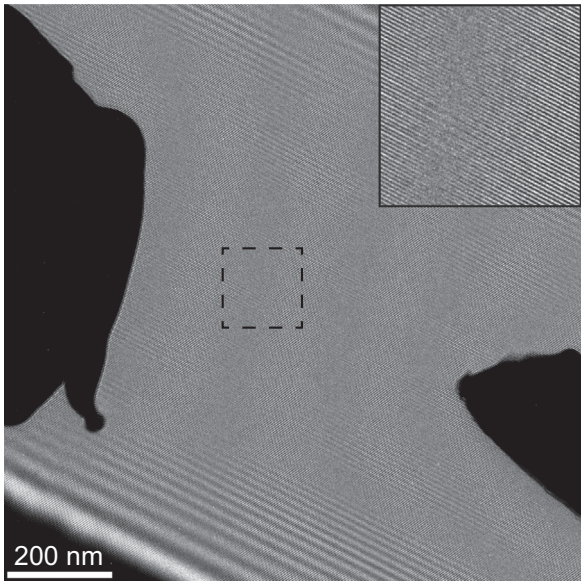

Fig. 2. Example of a continuously exposed electron hologram, which captures the projected electrostatic potential between the two metallic needles introduced in Fig. 1 (dark areas at the upper left and lower right corners). An electrical bias voltage of 5 V was applied between the needles in the form of a square wave with a frequency of 10 Hz. The hologram was acquired in an FEI Titan TEM operated at 300 kV in Lorentz mode with the objective lens switched off (in order to achieve an increased field of view). A voltage of 96 V was applied to a biprism wire positioned above the selected area aperture plane. The exposure time was 8 s. An enlargement of the moiré fringes is shown at the top right.

fringes. So long as the position of the specimen remains constant when the voltage is changed, the coarse fringes correspond to a phase difference of 2π between the two states and are imprinted on the amplitude of the total electron wave.

Fig. 3 shows the amplitude of the resulting electron wave, reconstructed using a standard fast Fourier transform based method [19] from the electron hologram shown in Fig. 2. The phase difference now takes the form of dark equiphase lines on an amplitude image of the needles and corresponds to a projection of the electrostatic potential in the electron beam direction, including the influence of the perturbed reference wave [6,20]. As the phase contours correspond to a difference between the two holograms, all contributions from imperfections in the imaging system of the microscope, such as those associated with the projector lenses of the microscope and the detector, are automatically removed.

3. Theory and discussion

This section provides details about the formation of double and continuous exposure electron holograms, by considering

Please cite this article as: V. Migunov, et al., Prospects for quantitative and time-resolved double and continuous exposure off-axis electron holography, Ultramicroscopy (2016), http://dx.doi.org/10.1016/j.ultramic.2016.08.010

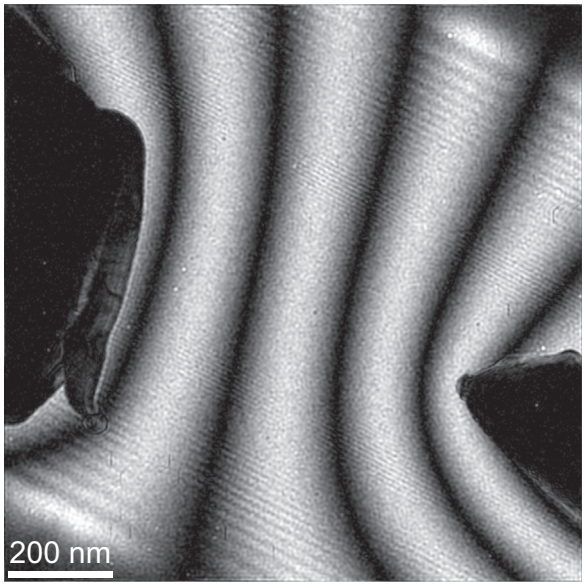

Fig. 3. Amplitude of the electron wave digitally recovered from the continuously exposed electron hologram shown in Fig. 2 using Fourier-transform-based digital reconstruction. The short range intensity variations at the top and bottom are due to Fresnel fringes from the edges of the biprism wire.

theoretical aspects and presenting comparisons with conventional off-axis electron holography.

3.1. Theory

In an idealised, conventional off-axis electron holographic setup, the object and reference waves interfere in the detector plane and give rise to an intensity distribution of the form

$$I(x) = |\sqrt{N/2}\, e^{-ik_0x} + \sqrt{N/2}\, a(x)e^{i\phi(x)}|^2 = \frac{N}{2}[1 + a^2(x) + 2a(x)\cos(k_0x + \phi(x))], \quad (1)$$

where $\sqrt{N/2}\, e^{-ik_0x}$ is the reference wave with transverse wave vector k_0 and $\sqrt{N/2}\, a(x)e^{i\phi(x)}$ is the object wave. The object wave experiences a position-dependent relative phase shift $\phi(x)$ and a position-dependent change in relative amplitude $a(x)$. N is the average number of electrons per pixel in the interference region in the absence of a specimen. The less-than-perfect degree of coherence between the reference and object waves can be taken into account by inserting a visibility factor V (*e.g.*, [21]). We do not consider at this stage loss of coherence due to the electron scattering within the specimen, which requires a more sophisticated statistical analysis to evaluate the local visibility [22]. The former equation then becomes

$$I(x) = \frac{N}{2}[1 + a^2(x) + 2\,Va(x)\cos(k_0x + \phi(x))]. \quad (2)$$

The intensity distribution in the final electron hologram is therefore a set of cosinusoidal fringes, whose positions are modulated by the object phase $\phi(x)$. Conventional electron holographic reconstruction proceeds by taking the Fourier transform of the intensity distribution, masking the sideband at $+k_0$, shifting this masked sideband back to the origin of Fourier space and then performing an inverse Fourier transform. This procedure is used to obtain the reconstructed wavefunction

$$\psi(x) = \frac{NV}{2}a(x)e^{i\phi(x)}. \quad (3)$$

When an electromagnetic fringing field extends into the vacuum region outside the object and perturbs the reference wave, which is then no longer a plane wave, its effect can be described in terms of a phase shift given by $\phi(x)-\phi(x + D)$, where D is the interference distance [9]. In the following treatment, in order to simplify the notation, it is assumed that the perturbed reference wave is already included in the phase $\phi(x)$.

In the simplest form of DEEH, the intensity distribution is a sum of two intensity distributions I_1 and I_2, each corresponding to its own object wave. Here, we assume that these object waves differ only in their phases, *i.e.*, the corresponding object waves are $a(x)e^{i\phi_1(x)}$ and $a(x)e^{i\phi_2(x)}$ (omitting normalisation factors). The recorded intensity distribution then takes the form

$$I(x) = I_1(x) + I_2(x) = \frac{N}{2}\left[1 + a^2(x) + Va(x)\cos(k_0x + \phi_1(x)) + Va(x)\cos(k_0x + \phi_2(x))\right] \quad (4)$$

and the wavefunction obtained from the reconstruction procedure described above is just the sum of the corresponding wavefunctions, *i.e.*,

$$\psi(x) = \psi_1(x) + \psi_2(x) = \frac{NV}{4}a(x)(e^{i\phi_1(x)} + e^{i\phi_2(x)}). \quad (5)$$

If the object phases are rewritten in the form

$$\phi_1(x) = \phi_0(x) + \phi(x), \quad \phi_2(x) = \phi_0(x)-\phi(x), \quad (6)$$

then the reconstructed wavefunction is

$$\psi(x) = \frac{NV}{2}a(x)\cos(\phi(x))e^{i\phi_0(x)} = A(x)\cos(\phi(x))e^{i\phi_0(x)}, \quad (7)$$

where the overall amplitude $A(x) = NVa(x)/2$. Taking the modulus of this wavefunction results in the expression

$$|\psi(x)| = A(x)|\cos(\phi(x))|. \quad (8)$$

Apart from the influence of the overall amplitude $A(x)$, $|\psi(x)|$ therefore corresponds to the (modulus of the) cosine of the DEEH phase $\phi(x) = \frac{1}{2}(\phi_1(x)-\phi_2(x))$. Moreover, the average phase $\phi_0(x) = \frac{1}{2}(\phi_1(x) + \phi_2(x))$, which is common to both object waves, is eliminated entirely.

Finally, if $A(x)$ is known, then the DEEH phase, modulo $\pi/2$, can in principle be recovered directly from the ratio $|\psi(x)|/A(x)$ according to the expression

$$\phi(x) = \arccos(|\psi(x)|/A(x)). \quad (9)$$

3.2. Noise

For the purpose of examining statistical errors in DEEH reconstructions, we assume for simplicity that the relative amplitude $a(x) = 1$, *i.e.*, we consider reconstruction in vacuum.

In conventional off-axis electron holography, shot noise, less-than-perfect beam coherence and detector noise all contribute to a statistical error in the phase of the reconstructed wavefunction, whose standard deviation is given by the expression [23] (see also Ref. [24])

$$\sigma_{\phi_0} \simeq \sqrt{\frac{2r}{NV_0^2\mathrm{DQE}}}, \quad (10)$$

where N is defined above, V_0 is the holographic fringe visibility that would be observed using an ideal pixelated detector, DQE is the detective quantum efficiency at the holographic interference fringe spacing and $r < 1$ is the ratio between the area enclosed by the sideband mask and the total area of Fourier space. This phase error applies to each pixel in the reconstructed wavefunction, where the pixel size matches that in the original electron hologram.

Please cite this article as: V. Migunov, et al., Prospects for quantitative and time-resolved double and continuous exposure off-axis electron holography, Ultramicroscopy (2016), http://dx.doi.org/10.1016/j.ultramic.2016.08.010

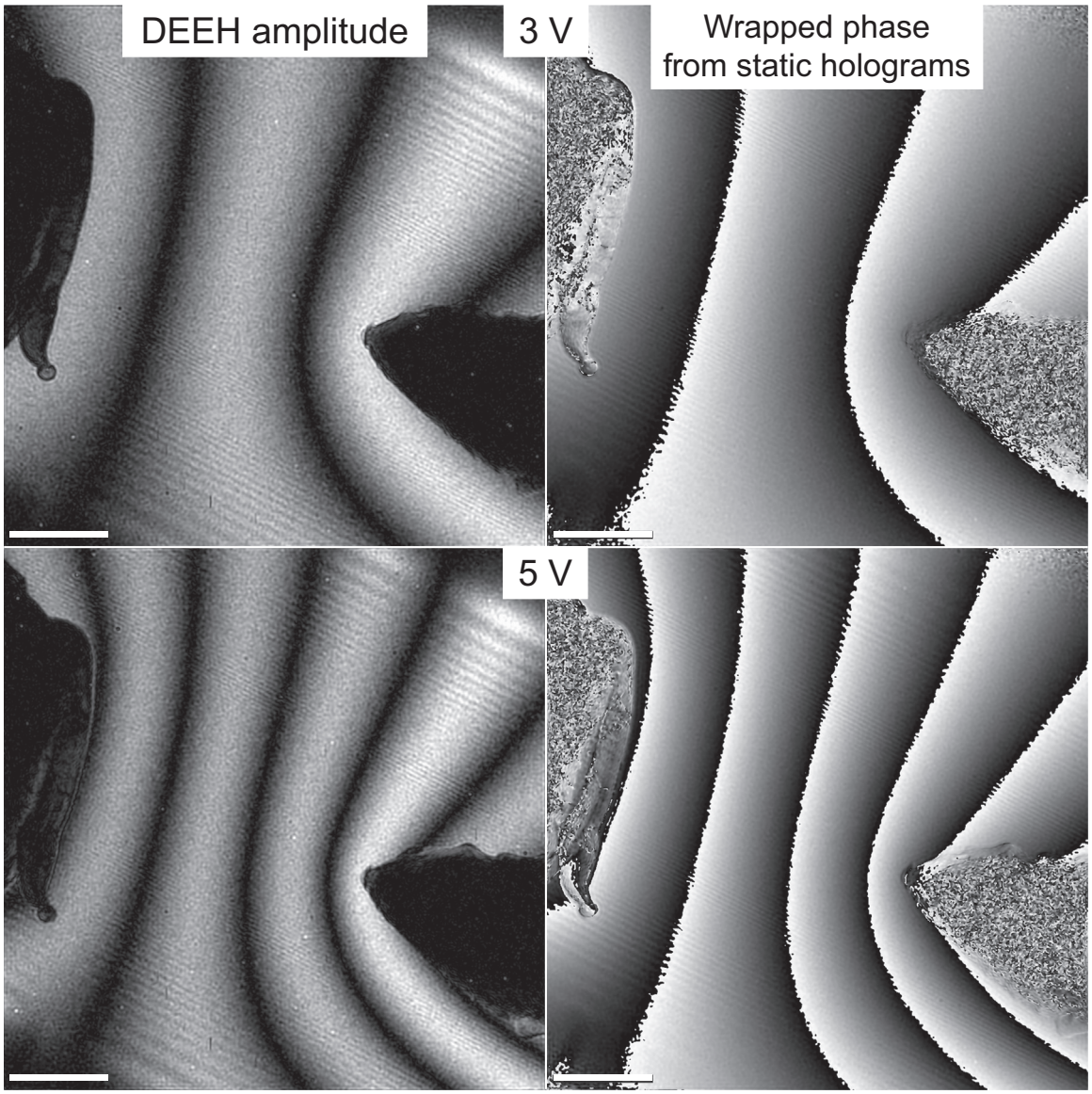

Fig. 4. Comparison between DEEH and conventional off-axis electron holography. The left column shows the amplitudes of double-exposed electron holograms for square wave bias voltages of 3 V (top) and 5 V (bottom) and a frequency of 100 kHz applied between the two needles. The right column shows wrapped phase images reconstructed from static off-axis electron holograms recorded using the same, but now constant, bias voltages. It should be noted that an offset of π was added to each of the phase images. All of the original holograms were acquired at the same microscope conditions as in Fig. 2. The scale bar is 200 nm.

In DEEH, in order to obtain an expression for the error in the phase $\phi = \frac{1}{2}(\phi_1 - \phi_2)$, we consider the propagation of errors associated with Eq. (9) in the form

$$\sigma_\phi^2 \approx \left(\frac{\partial \phi}{\partial |\psi|}\right)^2 \sigma_{|\psi|}^2 + \left(\frac{\partial \phi}{\partial A}\right)^2 \sigma_A^2, \tag{11}$$

where $\sigma_{|\psi|}^2$ and σ_A^2 are the variances in $|\psi|$ and A, respectively. If A can be estimated (for example, by averaging over a large area of the reconstructed wavefunction), then the contribution from the error in A will be negligible. By using Eq. (9), we then obtain the expression

$$\sigma_\phi \approx \frac{1}{\sqrt{1-(|\psi|/A)^2}} \frac{\sigma_{|\psi|}}{A}. \tag{12}$$

The error given by Eq. (12) diverges when $|\psi|/A = 1$, which corresponds to points where $\phi = n\pi$ and the error is amplified. This behaviour of the DEEH phase results from the form of the arccosine function. On the other hand, at points where $|\psi|/A = 0$, *i.e.*, $\phi = (2n + 1)\pi/2$ where n is an integer, the error in the DEEH phase becomes

$$\sigma_\phi \approx \frac{\sigma_{|\psi|}}{A}, \tag{13}$$

which is well-behaved and linearly proportional to $\sigma_{|\psi|}$. The points $|\psi|/A = 0$ correspond to zeros in contour maps produced by the method. Eq. (13) shows that well-behaved errors in the DEEH phase can be obtained in the vicinity of such points.

3.3. Comparison with standard off-axis electron holography

It follows from Eq. (8) that the amplitude of a double-exposed electron hologram contains phase information, whose error is influenced by the modulus operation. A direct comparison can be made with the wrapped phase of a standard off-axis electron hologram on the assumption that $\phi_1 = 0$ (*i.e.*, $\phi = \phi_2/2$). According to Eq. (6), minima in the DEEH amplitude then occur when

Please cite this article as: V. Migunov, et al., Prospects for quantitative and time-resolved double and continuous exposure off-axis electron holography, Ultramicroscopy (2016), http://dx.doi.org/10.1016/j.ultramic.2016.08.010

$\phi_2 = (2n + 1)\pi$. If ϕ_2 is measured using both techniques (from the DEEH amplitude and using standard off-axis electron holography), then the phase wraps in standard electron holography, which are located every 2π, will have a direct correspondence with DEEH amplitude minima with an offset of π.

In order to demonstrate this point experimentally, the two metallic needles described in Fig. 1 (see also Ref. [20]) were subjected to either a static or an alternating voltage difference. Fig. 4 shows the projected electrostatic potential between the needles imaged both "dynamically" by applying square pulses between the needles while recording a hologram using an exposure time that is much longer than the pulse length (DEEH) and "statically" using conventional off-axis electron holography. The zeros, in both cases representing projected equipotential lines, coincide with each other.

The following points outline the primary similarities and differences between the two approaches:

- As discussed above, both DEEH and conventional electron holographic phase maps can be used to observe equiphase lines of the electron wave. Nevertheless, standard off-axis electron holography measures the phase shift relative to a reference wave, whereas the DEEH amplitude contains information about the phase difference between two exposures (*i.e.*, ϕ_1 and ϕ_2), both relative to their reference waves. Assuming that one of the DEEH phases is zero, standard electron holography and DEEH will give a measure of the same quantity. Also, DEEH can be used when the phase difference between the two exposures (*i.e.*, $\phi_1 - \phi_2$) is of interest.
- The DEEH amplitude contains quantitative phase information, which is sampled by the modulus of the cosine function, meaning that the direction of the phase gradient cannot be determined using DEEH alone. This point is discussed further in Sections 4.3 and 5.2 below.
- Both methods suffer from rapidly changing phase variations, *i.e.*, more than 2π per holographic fringe. Such rapid phase changes result in spatial under-sampling of the phase shift and hence aliasing. The difference between the two techniques is again related to the fact that DEEH measures the phase difference between two temporally separated waves. Therefore, aliasing problems apply only to the phase difference $\phi_1 - \phi_2$ for DEEH. If one of the phase shifts in DEEH is constant, then the aliasing effect will be the same for both methods. Further information can be found elsewhere [25].
- Since both DEEH and conventional off-axis electron holography use Fourier-space reconstruction, the spatial resolution of both methods is limited by the size of the side-band filter used for reconstruction and the resolving power of the electron-optical system.
- Phase errors in DEEH depend on the value of the phase that is being measured (see Eqs. (12) and (13)). Well-behaved phase errors occur in the vicinity of zeros in a DEEH map and can be much greater away from such points.
- The phase sensitivity (smallest detectable phase shift) of DEEH is ultimately limited by the noise in the amplitude. Inside the specimen, since the amplitude is attenuated by absorption, there will be a further degradation of the phase sensitivity of DEEH. The same considerations will apply to spatial resolution, which is linked to phase sensitivity.
- The fact that DEEH records phase contours separated by π in the form of moiré fringes initially appears to suggest that the minimum detectable phase change required to form a single fringe is π. However, this is not the case, since the measured phase (independent of its value) is related to the DEEH amplitude by Eq. (9). This relationship results in possibilities for reconstructing the phase from the DEEH amplitude, as well as digital signal amplification, as discussed in Sections 4.2 and 4.3 below.
- Strong electric and magnetic fields may introduce image shifts,[1] which will result in artefacts in DEEH. In the case of conventional off-axis electron holography, such image shifts can be corrected by image alignment.

Although it may at first appear that DEEH offers no advantages over standard off-axis electron holography, the applicability of DEEH for measuring phases that oscillate in time provides significant benefits beyond traditional static or quasi-static cases. The basis of using double or continuous exposure electron holography for studies of time-dependent phase objects is presented in the following section.

3.4. Time-dependent object waves

In continuous exposure electron holography, a general scenario describes an object wave whose properties change during the exposure time T of an electron hologram. Once again, we limit ourselves to the case where only the object phase varies with time. We also assume that the object varies so slowly in time that the scattering problem can be treated quasi-statically (rather than explicitly considering it as a time-dependent problem). The recorded intensity distribution can now be written in the form of a time average integral

$$I(x) = \frac{1}{T}\int_0^T \mathrm{d}t\, I(x,t) = \frac{Na(x)}{T}\int_0^T \mathrm{d}t\, [1 + V\cos(k_0 x + \phi(x,t))]$$
$$= Na(x) + \frac{NVa(x)}{T}\int_0^T \mathrm{d}t\, \cos(k_0 x + \phi(x,t)). \tag{14}$$

The reconstruction procedure described above then yields the wavefunction

$$\psi(x) = \frac{A(x)}{T}\int_0^T \mathrm{d}t\, e^{i\phi(x,t)}. \tag{15}$$

For illustrative purposes, we consider object phases that have three specific time dependencies: (1) square wave, (2) sine wave and (3) triangle wave. The use of square and sine waves in dynamic experiments is discussed in Section 5.3. In each case, we assume that the period $2\pi/\omega$ with which the object phase oscillates in time is much shorter than the exposure time, *i.e.*, $2\pi/\omega \ll T$.

(1) *Square wave* – in this case (the only one that corresponds strictly to DEEH), the object phase alternates between two values, which, as above, we denote $\phi_0 - \phi$ and $\phi_0 + \phi$. As a result of the rapidity of the oscillation period, the total times for which the phase equals $\phi_0 - \phi$ and $\phi_0 + \phi$ are both very nearly equal to $T/2$. Hence, we obtain the same result as before, *i.e.*, the reconstructed wavefunction takes the form

$$\psi_{\mathrm{square}}(x) = A(x)\cos(\phi(x))e^{i\phi_0(x)} \tag{16}$$

and all quantities are defined as above.

(2) *Sine wave* – in this case, the time integral can be split into $\omega T/2\pi$ periods, during each of which the phase varies sinusoidally between its extreme values of $\phi_0 - \phi$ and $\phi_0 + \phi$. The integral is now

$$\frac{1}{T}\int_0^T \mathrm{d}t\, e^{i\phi(x,t)} = \frac{1}{T}\frac{\omega T}{2\pi}\int_{-\pi/\omega}^{\pi/\omega} \mathrm{d}t\, e^{i(\phi_0(x)+\phi(x)\sin\omega t)}$$
$$= \frac{1}{T}\frac{\omega T}{2\pi}e^{i\phi_0(x)}\frac{2\pi}{\omega}J_0(\phi(x)) = e^{i\phi_0(x)}J_0(\phi(x)), \tag{17}$$

where J_0 is the zeroth-order Bessel function. The wavefunction

[1] More precisely, strong fields produce beam tilts. Together with aberrations or as a result of other artefacts, they may then cause image shifts.

Please cite this article as: V. Migunov, et al., Prospects for quantitative and time-resolved double and continuous exposure off-axis electron holography, Ultramicroscopy (2016), http://dx.doi.org/10.1016/j.ultramic.2016.08.010

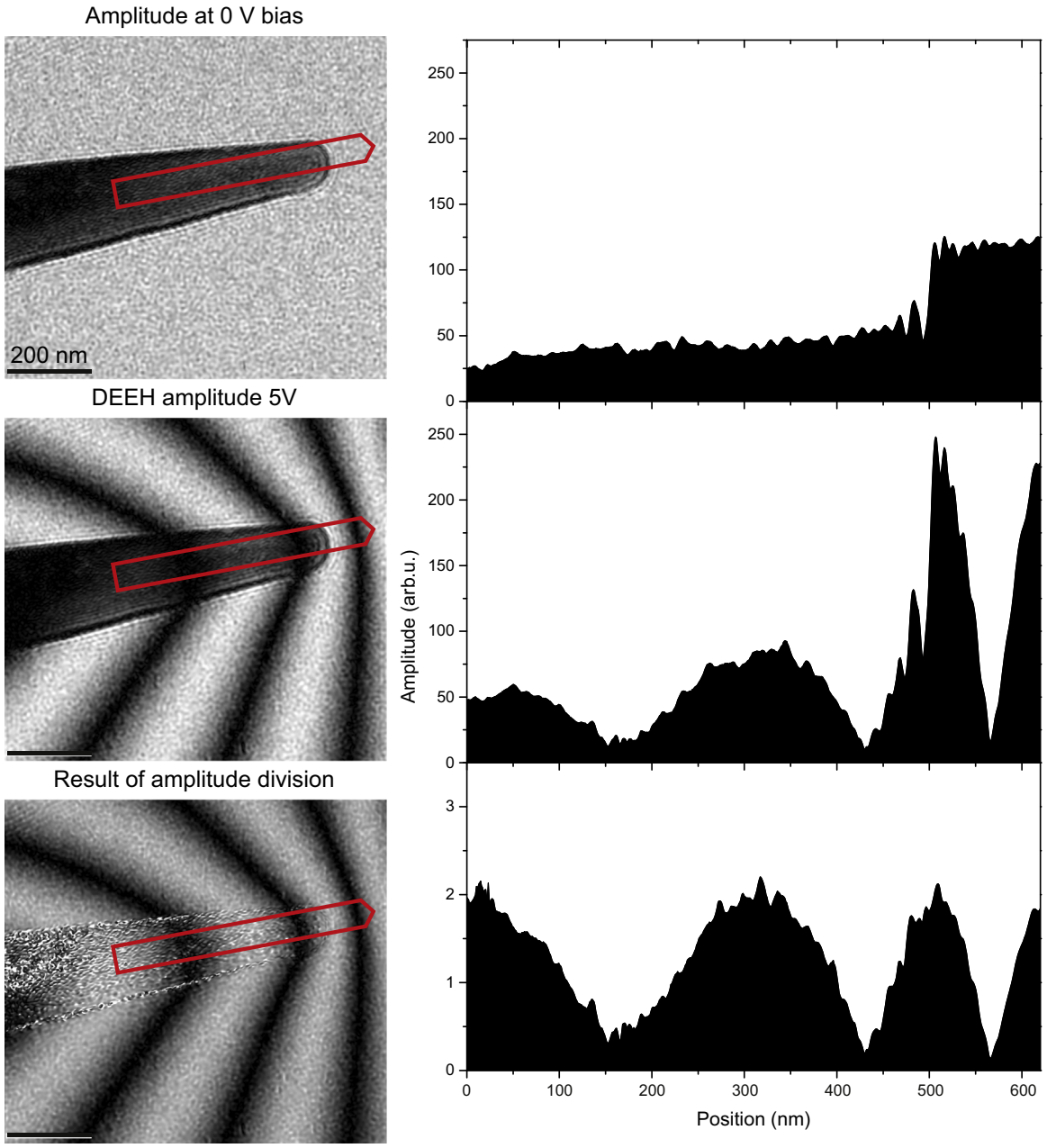

Fig. 5. Illustration of the removal of the effect of absorption inside a specimen from a DEEH amplitude image. Reconstructed amplitude images (left) were recorded from a metallic needle with no bias voltage applied (top), from a double-exposed electron hologram with biases of 0 and 5 V (middle) and (bottom) after using the unbiased image (top) to correct for the amplitude change in the DEEH image (middle), as described in the text. The line profiles on the right show the intensity along the red boxes marked in each image on the left. The integration widths correspond to the dimensions of the boxes. The scale bar is 200 nm. (For interpretation of the references to colour in this figure legend, the reader is referred to the web version of this article.)

now takes the form

$$\psi_{\text{sine}}(x) = A(x)J_0(\phi(x))e^{i\phi_0(x)} \tag{18}$$

and exhibits a Bessel-function dependence on the phase $\phi(x)$.

(3) *Triangle wave* – in this case, the time integral can be split into $\omega T/\pi$ half-periods, during each of which the phase varies linearly between $\phi_0-\phi$ or $\phi_0+\phi$. We now obtain the expression

$$\frac{1}{T}\int_0^T \mathrm{d}t\; e^{i\phi(x,t)} = \frac{1}{T}\frac{\omega T}{\pi}\int_{-\pi/2\omega}^{\pi/2\omega}\mathrm{d}t\; e^{i(\phi_0(x)+2\phi(x)\omega t/\pi)} = \frac{1}{T}\frac{\omega T}{\pi}e^{i\phi_0(x)}\frac{\pi}{\omega}\frac{\sin(\phi(x))}{\phi(x)} = e^{i\phi_0}\mathrm{sinc}(\phi(x)). \tag{19}$$

Hence, the wavefunction takes the form

$$\psi_{\text{triangle}}(x) = A(x)\mathrm{sinc}(\phi(x))e^{i\phi_0(x)} \tag{20}$$

and exhibits a sinc-function dependence on the phase $\phi(x)$.

The above three time dependencies are ordered hierarchically, in the sense that they result in an increasingly rapid decay of the wavefunction's envelope with $|\phi|$. More specifically, the envelope of $\cos(\phi)$ (for the square wave) does not decay, that of $J_0(\phi)$ (for the sine wave) decays as $|\phi|^{-1/2}$ and that of $\mathrm{sinc}(\phi)$ (for the triangle wave) decays as $|\phi|^{-1}$. Physically, this behaviour is linked to the different ways in which the electron holographic fringes move during the exposure time.

(4) *Arbitrary periodic wave* – if no assumptions are made about the time dependence of the object phase, other than it being

Please cite this article as: V. Migunov, et al., Prospects for quantitative and time-resolved double and continuous exposure off-axis electron holography, Ultramicroscopy (2016), http://dx.doi.org/10.1016/j.ultramic.2016.08.010

(i) independent of position and (ii) periodic with period $2\pi/\omega \ll T$, then it can be written in the form

$$\phi(x, t) = \phi_0(x) + \phi(x)f(t), \tag{21}$$

where $f(t)$ is an arbitrary periodic function with an average value of zero. In this general case, the time integral is

$$\frac{1}{T}\int_0^T \mathrm{d}t\ e^{i\phi(x,t)} = \frac{e^{i\phi_0(x)}}{T}\int_0^T \mathrm{d}t\ e^{i\phi(x)f(t)} = e^{i\phi_0(x)}Z[f](\phi(x)), \tag{22}$$

where the functional $Z[f](\phi(x))$ is a non-trivial complex function of $\phi(x)$, whose form depends on that of $f(t)$. This situation is distinctly different from the cases above, for which $Z[f]$ was real. Here, the consequence is that the reconstructed wavefunction will contain, in addition to the average phase $\phi_0(x)$, a non-trivial phase $\arg Z[f](\phi(x))$. However, some simplifications are again possible for special cases. By expanding $f(t)$ in the form of a Fourier series

$$f(t) = \sum_{n=1}^{\infty} f_n^c \cos(n\omega t) + \sum_{n=1}^{\infty} f_n^s \sin(n\omega t), \tag{23}$$

it can be shown that $Z[f]$ is real if $f(t)$ is an odd function (that is, if $f_n^c = 0$ for all n) or if $f(t)$ contains only odd harmonics (that is, if $f_n^c = f_n^s = 0$ for n even). (These conditions also hold when a time translation is necessary for $f(t)$ to possess one of these properties. For example, it holds for a cosine wave, which is an even function that is rendered odd upon a quarter-period translation.). In all such cases, the reconstructed wavefunction takes the form

$$\psi(x) = A(x)R[f](\phi(x))e^{i\phi_0(x)}, \tag{24}$$

where the functional $R[f](\phi(x))$ is real.

4. Extension of the technique through digital analysis

4.1. Approaches for removing absorption

As mentioned above, in vacuum DEEH will produce very similar results to conventional electron holographic phase images, albeit initially displayed in the form of the absolute value of the cosine of

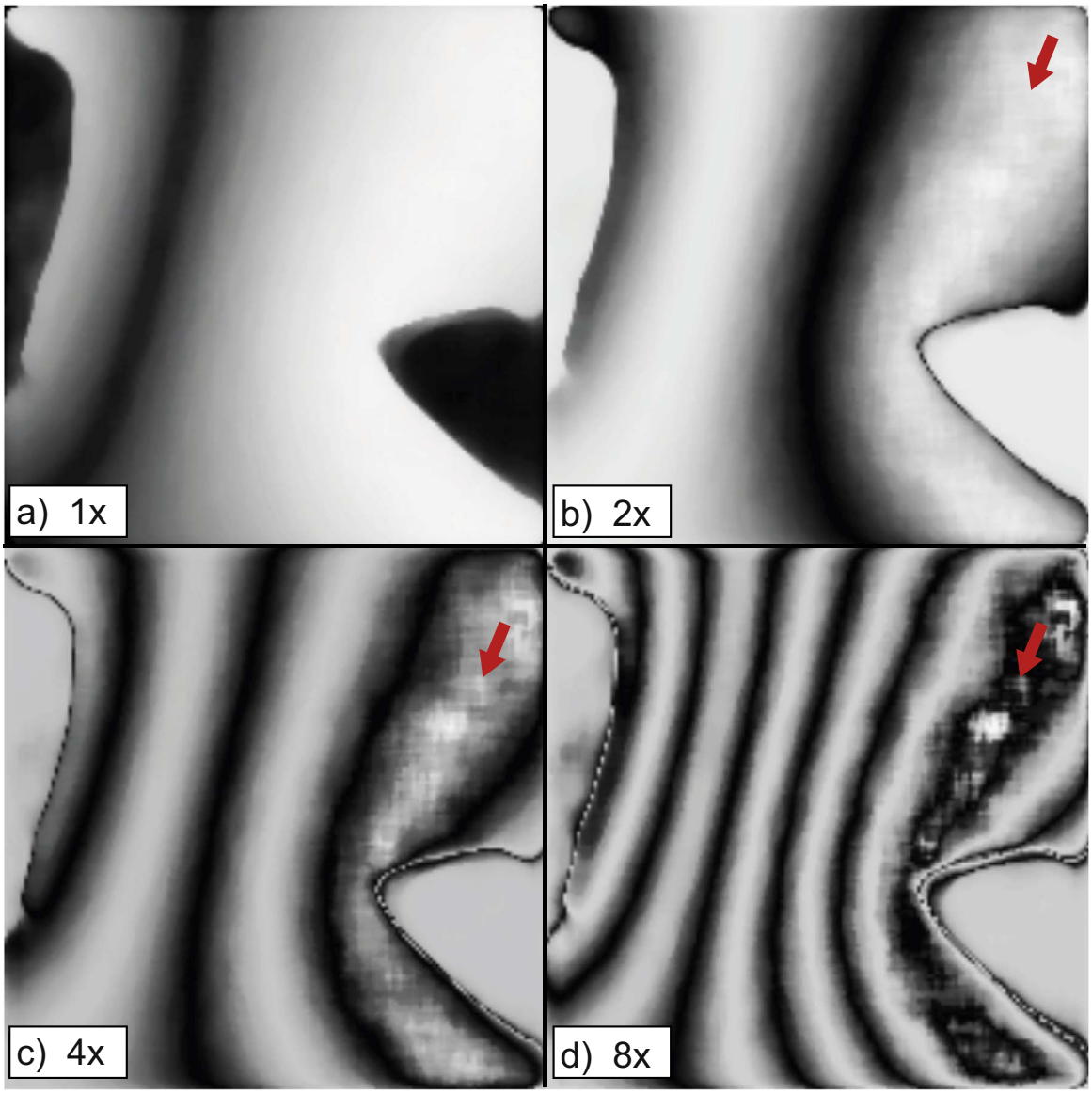

Fig. 6. Illustration of phase amplification in vacuum in DEEH. (a) Original reconstructed DEEH amplitude of two metallic needles with a square wave bias of amplitude 1 V applied between them. The original hologram was acquired at the same microscope conditions as in Fig. 2. b–d) 2, 4 and 8 times amplified phase contour maps calculated using Eqs. (27a), (27b) and (27d), respectively. The influence of absorption on the phase recorded inside the needle was not taken into account here. (For interpretation of the references to color in this figure, the reader is referred to the web version of this article.)

Please cite this article as: V. Migunov, et al., Prospects for quantitative and time-resolved double and continuous exposure off-axis electron holography, Ultramicroscopy (2016), http://dx.doi.org/10.1016/j.ultramic.2016.08.010

the phase. In contrast, in the presence of a specimen the amplitude of a DEEH can be described in terms of a combination of absorption $A(x)$ and the phase difference term $|\cos(\phi(x))|$ (see Eq. (8)). In principle, if the absorption inside the specimen $A(x)$ is known, then it is possible to recover the phase from the amplitude of the reconstructed electron wave. This separation can be performed digitally by division of the amplitude of the double-exposed hologram by the amplitude recovered from a conventional electron hologram of the same object recorded without changing the illumination conditions (including the tilt of the sample with respect to the electron beam).

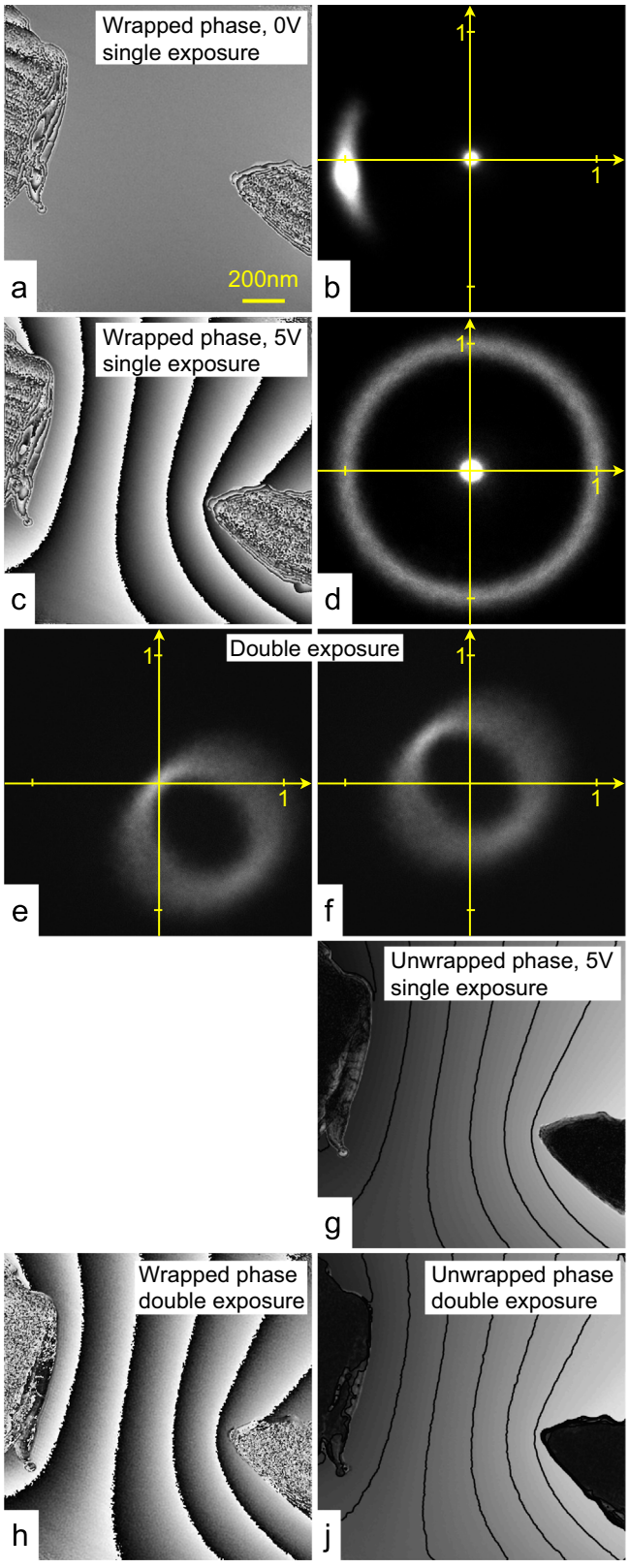

Fig. 5 illustrates the application of this approach to recover the phase term for an electrically biased needle. In this example, the DEEH amplitude (acquired by using a bias switched between 5 and 0 V, as shown in the middle panel of Fig. 5) was divided by the amplitude of the needle acquired at zero bias (top panel). The resulting amplitude, which contains the pure modulus of the cosine of the phase difference between biases of 0 and 5 V, is shown in the bottom panel. This image now shows the effect of the bias inside the needle. It does, however, have increased noise inside the needle and contains some artefacts, both at its edge and in the regions where the specimen thickness is highest.

The removal of absorption improves the applicability of DEEH for imaging electrostatic potentials and magnetic fields inside specimens, as well as in vacuum. Significantly, the type of time dependence of the object wave in double or continuous exposure electron holography does not matter if the amplitude of the wave remains constant, meaning that the method can be applied to any oscillatory phase change (including sinusoidal and triangle waves) inside the specimen.

4.2. Phase amplification

In DEEH, phase shifts that are smaller than 2π cannot be visualised directly since they result in either no moiré fringes or only one moiré fringe. Amplification of the phase is then required and can be useful for live visualisation of measured equiphase surfaces. Although one of the original papers on DEEH suggested that two-times phase amplification can be achieved by superimposing two holograms taken with the object in opposite positions with respect to the biprism [12], the discussion here is dedicated to phase amplification approaches that can be applied to any double or continuous exposure electron holograms using digital processing.

The method that we describe below is based on the trigonometric expansion of the cosine of multiples of an argument, *i.e.*, $\cos(nx)$, where n is an integer amplification factor [26]. For any positive integer n, $\cos(nx)$ can be expanded by using Chebyshev polynomials $T_n(y)$ as follows [27]:

$$\cos(nx) = T_n(\cos(x)),\ T_n(y) = \sum_{k=0}^{\lfloor n/2 \rfloor} \binom{n}{2k} (y^2-1)^k y^{n-2k}. \tag{25}$$

Given that the phase depends on the reconstructed amplitude and can be written as $|\psi| = A(x)|\cos(\frac{\phi(x)}{2})|$ (see Eq. (8)), Eq. (25) can

Fig. 7. Illustration of reconstruction of the phase from a DEEH using the Argand diagram method described in the text. a) Phase and b) Argand diagram determined from the complex wave reconstructed from a single exposure off-axis electron hologram recorded using a bias of 0 V between two metallic needles. The bright area in the centre of the Argand diagram (*i.e.*, at $0+0i$) represents areas where there is little intensity (e.g., at the positions of the needles themselves). The bright spot at the left represents the mostly constant amplitude and phase between the needles. The arc extending from this bright spot results from a small variation in phase in vacuum. c) Phase and d) Argand diagram determined from a similar single exposure off-axis electron hologram recorded using a bias of 5 V between the needles. e) Argand plot of the DEEH complex wave reconstructed from Fig. 2 after normalisation using the complex wave reconstructed from a single exposure off-axis electron hologram recorded at 0 V bias. f) The same Argand plot now after subtracting the complex value at the centre of the circle $0.354–0.354i$ from the complex wave reconstructed from Fig. 2. g) Unwrapped phase reconstructed from the single exposure off-axis electron hologram recorded at 5 V bias, overlaid with the corresponding TEM bright-field image and phase contours. h) Wrapped phase and j) unwrapped phase determined from the shifted complex wave corresponding to the shifted Argand plot in (f). The phase (j) is overlaid with a TEM bright-field image and phase contours.

Please cite this article as: V. Migunov, et al., Prospects for quantitative and time-resolved double and continuous exposure off-axis electron holography, Ultramicroscopy (2016), http://dx.doi.org/10.1016/j.ultramic.2016.08.010

be rewritten in the form

$$A_n = \cos(n\phi) = \sum_{k=0}^{\lfloor n/2 \rfloor} \binom{n}{2k} \left(\frac{|\psi|^2}{A(x)^2} - 1\right)^k \left(\frac{|\psi|^2}{A(x)^2}\right)^{\frac{n}{2}-k}. \quad (26)$$

Since the phase is wrapped by the absolute value of a cosine function and not just a cosine, phase amplification should be performed using ψ^2 rather than $|\psi|$ itself. As a result, the amplification factor n is restricted to even positive integers. For example:

$$\cos(2\phi(x)) = 2\cos^2(\phi(x)) - 1 \quad (27a)$$

$$\cos(4\phi(x)) = 8\cos^4(\phi(x)) - 8\cos^2(\phi(x)) + 1 \quad (27b)$$

$$\cos(6\phi(x)) = 32\cos^6(\phi(x)) - 48\cos^4(\phi(x)) + \quad (27c)$$

$$18\cos^2(\phi(x)) - 1\cos(8\phi(x)) = 128\cos^8(\phi(x)) - 256\cos^6(\phi(x)) + 160^4(\phi(x)) - 32\cos^2(\phi(x)) + 1. \quad (27d)$$

These formulae can be applied to a reconstructed amplitude image to amplify a weak phase signal.

In order to demonstrate phase amplification on experimental DEEH amplitude images, we acquired off-axis electron holograms of the two metallic needles while applying an electrical bias between them with an amplitude of 1 V in the form of a square wave, as described in Section 2 and shown schematically in Fig. 1. The original DEEH amplitude image is shown in Fig. 6a. Amplified phase contour maps, calculated using Eqs. (27a), (27b) and (27d), are shown in Figs. 6b–d. The approach can be seen to work successfully for amplification values of up to 8. Although only 8 times amplification is demonstrated here, further amplification is possible, subject to the influence of noise in the experimental image, which makes contours corresponding to maxima in the original DEEH amplitude (see, e.g., the contour marked by the red arrow in Fig. 6) less visible after each further amplification step. This loss of information occurs most prominently at maxima in the DEEH amplitude as a consequence of a significant increase in noise at these positions when compared to the rest of the image (see Section 3.2 and Eq. (13) for a detailed description of DEEH noise). Nevertheless, all other information is preserved and amplification can be performed successfully in regions that do not coincide with maxima.

An alternative to amplification is direct retrieval of the phase difference from the amplitude, which is addressed in the following section. Amplification has an advantage over unwrapping when online visualisation of weak phase shifts is required. With modern computation capacities, the reconstruction of DEEH amplitudes and subsequent amplification can be performed effectively live. It is worth mentioning that the phase amplification approach described above can only be performed for the case of a square wave dependence of the phase on time. Phase amplification can be applied inside the specimen after removing absorption by dividing the DEEH amplitude by the amplitude of a single off-axis electron hologram.

4.3. Phase unwrapping from the reconstructed amplitude

In this section, we describe two approaches that can be used to reconstruct the phase difference between two states of a system from double-exposed electron holograms. For illustrative purposes, the two states in the discussion correspond to electrical biases of 0 and 5 V applied to the two electrically biased needles that are described in Section 3.3.

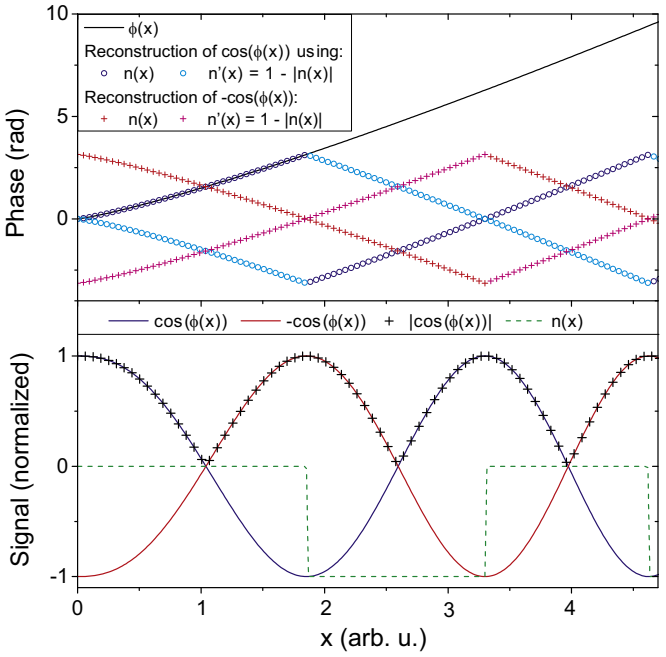

Fig. 8. Illustration of recovery of the one-dimensional phase $\phi(x)$ from the DEEH amplitude $|\cos(\phi(x))|$. The top panel shows the original phase (black solid line) and variants of its recovery (circles and crosses). The bottom panel shows the amplitude signal (black crosses) and variants of its inversion (blue and red solid lines). Depending on the definition of $n(x)$ (green dashed line in lower graph) and on the inversion of the cosine function (red and blue solid lines), the result of phase recovery can either match the input signal (blue circles in the upper graph) or not provide a match (cyan circles and crosses). (For interpretation of the references to color in this figure legend, the reader is referred to the web version of this article.)

The first approach is based on Argand diagram analysis and is described in Fig. 7. Fig. 7a–d shows reconstructed phase images and Argand diagrams determined from complex wavefuctions reconstructed from single exposure off-axis electron holograms recorded with applied biases between the needles of 0 V (Fig. 7a and b) and 5 V (Fig. 7c and d). The aim is to reconstruct the phase difference between these two states from a DEEH recorded using a bias that oscillates between 0 and 5 V, in this case at a frequency of 10 kHz.

As the phase at 0 V bias (Fig. 7a) is almost constant, the corresponding Argand diagram (Fig. 7b) consists of a bright spot on the left representing an area of almost constant amplitude and phase, with a short arc arising from small variations in the phase across the field of view. These phase variations may arise from small amounts of charging on the edges of the needles. The areas of the needles themselves have an amplitude close to zero and give rise to the bright spot at the origin of the Argand diagram in Fig. 7b.

The phase at 5 V bias (Fig. 7c) consists approximately of a ramp, which is wrapped (in phase) 5 times across the image. As a result, its Argand diagram (Fig. 7d) takes the form of a circle that has constant amplitude, but phases that are distributed over the full angular range of 0–2π. The desired phase difference between the two biased states is therefore expected to be almost the same as the phase for the 5 V state (Fig. 7c), since the phase at 0 V bias (Fig. 7a) is almost constant.

The Argand plot of the electron wave reconstructed from the double-exposed electron hologram (Fig. 7e) is also approximately a circle, but is now offset such that it passes through the origin. This is a result of interference between the two sets of fringes in

the DEEH hologram causing the fringe amplitude to be modulated by a cosine function (see Section 3.1). However, a circle forms only if the amplitude and phase of the double-exposed electron hologram are normalised by dividing the DEEH wave by the wave reconstructed from a static off-axis electron hologram of the same area. In the ideal case, the circle will have a radius of 0.5. The formation of a circle assumes that the double-exposed hologram consists of the superposition of two single-exposed holograms and that one of these single-exposed holograms is used for normalisation. Deviations from these assumptions, such as different amounts of charging or blurring of the DEEH due to a non-square-wave bias, will cause the position of the circle to change over the field of view and result in blurring, such as that seen in Fig. 7e.

In order to retrieve the phase from a DEEH using the Argand plot method, the points in the Argand diagram from the DEEH wave (Fig. 7e) must be shifted so that the centre of the circle coincides with the origin of the plot, so as to give an image with constant amplitude and varying phase. The centre of the circle has an amplitude of 0.5, but its phase depends on the change between the phase of the fringes in the DEEH and the phase in the static hologram used for normalisation. In Fig. 7e, the centre of the circle is found to be at $0.354–0.354i$. Subtracting this value from the complex wave gives the Argand diagram shown in Fig. 7f, which consists of (approximately) a circle, now centred at the origin. The reconstructed amplitude is now approximately constant. The phase (Fig. 7h and j) represents the difference in phase between the two states of the DEEH. The unwrapped phase, which is shown with equiphase contours superimposed in Fig. 7j, is in good agreement with the phase unwrapped from a conventional off-axis electron hologram recorded at a constant bias of 5 V (Fig. 7g, derived from Fig. 7c and with equiphase contours superimposed).

The second method that we propose for retrieval of the phase from a DEEH relies on direct unwrapping of the DEEH amplitude $|\psi(x)|$, whose relationship to half of the phase difference ϕ is known and takes the form $|\psi(x)| = A(x)|\cos(\phi(x))|$. However, the cosine function is even and wraps $\phi(x)$ over the interval $(0; 2\pi]$, which, as in conventional off-axis electron holography, results in a sign ambiguity and 2π phase wrapping. The modulus of the cosine imposes a periodicity of $(0; \pi]$, which results in an additional π ambiguity (*i.e.*, $|\cos(\phi(x)) = |\cos(-\phi(x))| = |\cos(\phi(x) + n\pi)|$, where n is

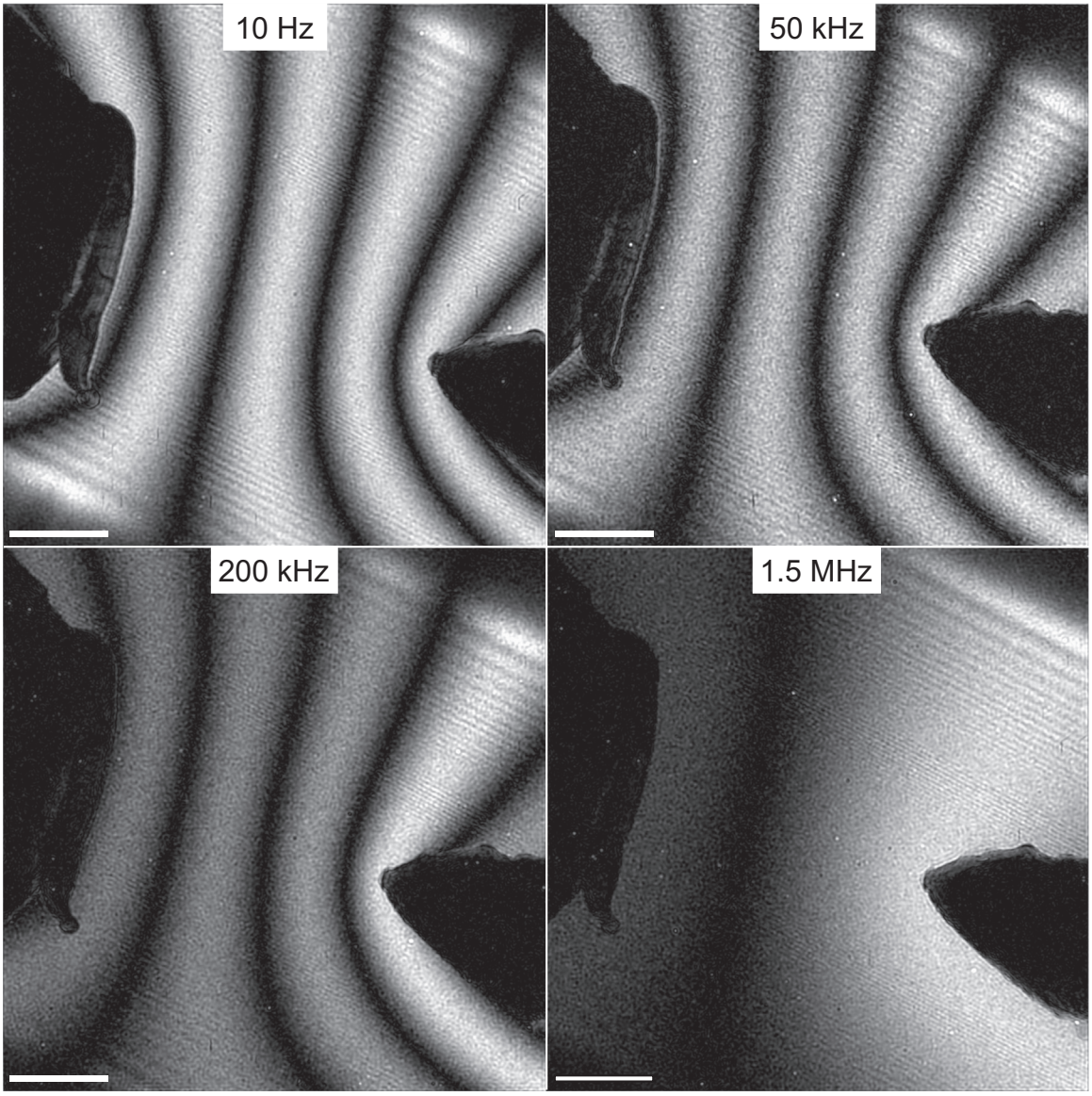

Fig. 9. Frequency dependence of a double-exposed electron hologram for a square wave with an amplitude of 5 V applied between the needles. The original holograms were acquired using the same microscope conditions as in Fig. 2. No signal transformation is visible for frequencies up to 50 kHz. A modulation in signal shape (*i.e.*, a variation in intensity across the contours) is observed at 200 kHz. A decreased number of contours is observed at 1.5 MHz. The scale bar is 200 nm.

Please cite this article as: V. Migunov, et al., Prospects for quantitative and time-resolved double and continuous exposure off-axis electron holography, Ultramicroscopy (2016), http://dx.doi.org/10.1016/j.ultramic.2016.08.010

an integer). In conventional off-axis electron holography, the sign ambiguity is resolved by choosing one or the other of the two conjugate images (waves) [28]. This selection is usually based either on geometrical criteria (*i.e.*, the relative position of the biprism and the specimen) or, more pragmatically, by ensuring that the phase shift associated with the mean inner potential (MIP) of the specimen is positive. In DEEH, the first approach cannot be used, since the reconstruction step is performed before determining the phase from the DEEH amplitude. The MIP criterion can be used so long as the DEEH map contains MIP information and an area where the MIP or specimen thickness is known to increase, for example at a specimen edge. If an external stimulus is applied during the acquisition of a DEEH (as in Section 2), then the MIP contribution to the phase cancels out. The sign ambiguity problem can then only be resolved by the use of prior knowledge. For example, the same voltage can be applied statically and a conventional off-axis electron hologram can be acquired and used to determine the sign of the phase in the final DEEH reconstruction.

In order to reconstruct the phase from the DEEH amplitude, one can use the method proposed by Tay and co-workers, who used the following equation to reconstruct the phase from a cosinusoidal fringe pattern [29]:

$$\phi(r) = 2(-1)^{n(r)}\arctan\left(\sqrt{\frac{1-A(r)}{1+A(r)}}\right), \tag{28}$$

where $A(r)$ is the amplitude of the DEEH and $n(r)$ is the maximum

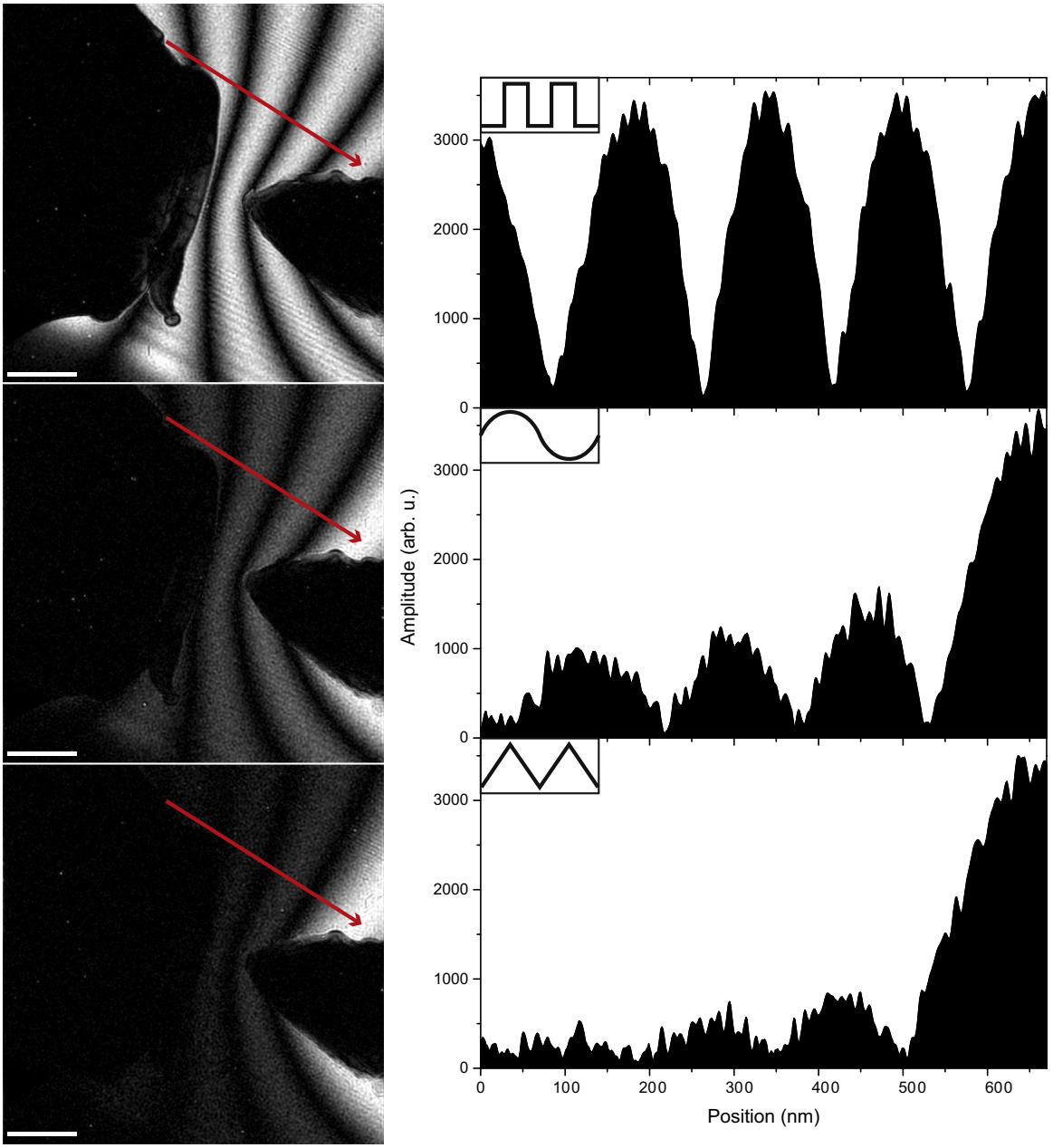

Fig. 10. Pulse-shape-dependence of the amplitude reconstructed from continuously exposed off-axis electron holograms. All of the applied waves have an amplitude of 5 V and a frequency of 5 Hz. The original holograms were acquired using the same microscope conditions as in Fig. 2. The reconstructed amplitude images are shown on the left. Corresponding line profiles extracted along the lines marked in the images are shown on the right. The waves applied between the needles (square, sine and triangle) are shown as insets. The intensity of the contours decays for the sine and triangle waves. The strongest decay is observed for the triangle wave, as discussed in Section 3.4. The scale bar is 200 nm.

Please cite this article as: V. Migunov, et al., Prospects for quantitative and time-resolved double and continuous exposure off-axis electron holography, Ultramicroscopy (2016), http://dx.doi.org/10.1016/j.ultramic.2016.08.010

detection function, which is defined to be zero in the reference region and either $n-1$ across a minimum or $n+1$ across a maximum. As an example, Fig. 8 shows the reconstruction of the phase $\phi(x) = x^{1.2}$ from $|\cos(\phi(x))|$. The following steps summarise the reconstruction procedure:

1. Detection of local minima.
2. Inversion of every second region between local minima. This step recovers $\cos(\phi(x))$ from $|\cos(\phi(x))|$. The result is shown in the lower panel in Fig. 8. Black crosses correspond to the original signal, while the blue solid line shows inversion of every second region between local minima.
3. Detection of local maxima and minima in the resulting function $\cos(\phi(x))$.
4. Determination of the function $n(x)$ by setting $n(x)$ to 0 at e.g., $x=0$, increasing $n(x)$ by 1 after a local maximum is crossed (refer to the blue line in Fig. 8) and decreasing $n(x)$ by 1 after a local minimum is crossed. (The details of the procedure are described elsewhere [29].) See the green dashed line in the lower panel of Fig. 8.
5. Calculation of the phase according to Eq. (28). The result is shown as blue circles in the top panel of Fig. 8.

As inversion of $|\cos(\phi(x))|$ (step 2) and the definition of $n(x)$ (step 4) cannot be absolute, these steps impose some ambiguity on the results of phase recovery. Inversion can result in $\pm\cos(\phi(x))$ and step 4 can result in either $n(x)$ (as shown in Fig. 28) or $n'(x) = 1-|n(x)|$. All possible results of phase recovery are summarised in the top panel of Fig. 8. In addition to the sign ambiguity (blue and cyan circles), an additional π ambiguity is possible (red and magenta crosses). Of the 4 possible reconstructions, only one (blue circles) delivers the correct result. However, given that the relative phase shift is of interest, only the sign has to be resolved using prior knowledge.

This algorithm can be extended to two-dimensional experimental images. A straightforward approach would be to implement the algorithm line-by-line. However, more sophisticated methods, such as finding local minima and maxima by thresholding combined with image processing, can be used to optimise recovery. In addition, as a result of noise in experimental images,

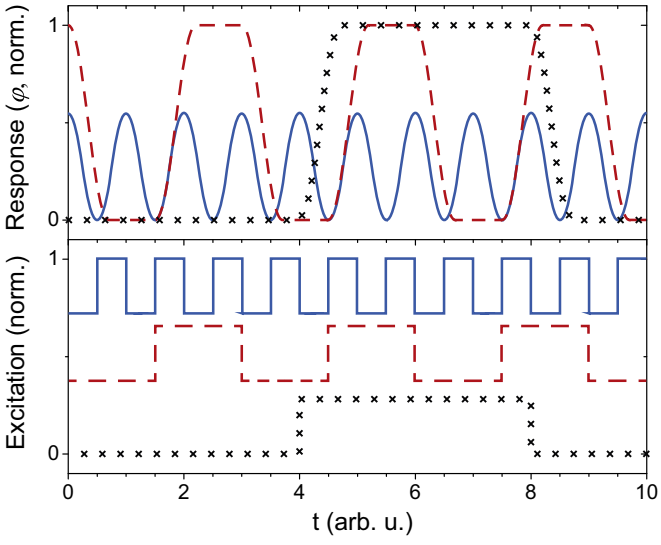

Fig. 11. Schematic representation of frequency-dependent pulse modulation. The lower panel shows applied pulses of different frequency as a function of time *t*. The traces are shifted vertically with respect to one another. The top panel shows the possible response of the system to each applied pulse sequence. See text for details. (For interpretation of the references to color in this figure legend, the reader is referred to the web version of this article.)

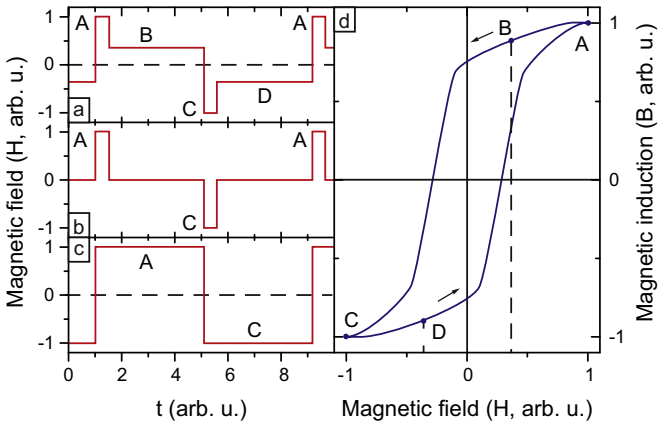

Fig. 12. Schematic representation of a quasi-static magnetic switching experiment. Panels (a-c) show possible sequences of applied pulses as a function of time *t*. Panel (d) shows the hysteresis curve of the specimen. The applied pulses can be used to access: (a) arbitrary points B and D in the hysteresis cycle; (b) remanent states and (c) saturated states.

renormalisation of the segments between local minima and maxima may be required, since their values may be different from 0 and 1, respectively, as required by Eq. (28). It is also worth mentioning that unwrapping of the amplitude in the specimen region would require the removal of absorption, as discussed in Section 4.1. Although phase retrieval using this approach from experimental DEEH maps was attempted, the results were not of sufficient quality to be presented in this paper.

5. Prospects for future experimental development

In the above sections, we presented double and continuous exposure holography and its application to the measurement of electrostatic fields that do not go beyond the possibilities of standard off-axis electron holography. However, the primary advantage of DEEH is the prospect of its application to dynamic experiments.

In off-axis electron holography, temporal resolution is often limited by the performance of detectors. As a result of the development of direct electron detection cameras, temporal resolution can now be pushed to frame rates exceeding a few kHz [17]. Another approach is dynamic and ultrafast TEM, which involves pulsing the electron gun with a laser to emit ultra-short electron pulses [30]. However, such experiments cannot yet be combined with off-axis electron holography, since the required coherence has not been achieved using laser-induced electron emission in the TEM.

Although DEEH does not itself offer a direct improvement in temporal resolution, it is able to capture phase differences between two states of a system, between which the separation in time can be as small as a few fs (or less). A limitation is that the total exposure remains as long as in conventional off-axis electron holography, meaning that the method is limited to fully reversible processes that can be repeated many times during a typical exposure time of between a few ms and a few tens of seconds. The following sections describe initial experiments that have been performed to test the technique by using different pulse shapes and frequencies. Examples of future experiments that promise to benefit from DEEH are then presented in Section 5.3.

5.1. High frequency experiments

In order to demonstrate that DEEH can be used for high frequency experiments, we used the system of two electrically biased

needles that was described in Section 2 and shown schematically in Fig. 1. A square wave was applied between the needles with an amplitude of 5 V at frequencies of between 1 Hz and 2 MHz. At all frequencies, holograms could be formed without any loss of coherence. However, the reconstructed amplitudes showed that at higher frequencies the signal was partially lost (see Fig. 9). Fig. 9a and b shows projected equipotential contours that are similar to those measured using conventional off-axis electron holography (see Section 3.3 and Fig. 4 for comparison), with no change in signal amplitude or shape up to 50 kHz. However, in Fig. 9c, which shows a reconstruction performed for a frequency of 200 kHz, the intensity distribution across the contours is not even and the contour at the apex of the right needle is brighter than the others. Moreover, at 1.5 MHz (Fig. 9d), not only is the intensity redistributed between the contours, but the total number of equiphase contours has decreased by approximately a factor of 5. The decrease in the number of contours corresponds to an attenuation of the field. The appearance of a brighter contour is a sign of transformation of the signal, *i.e.*, the square wave sent into the system transforms into a smoother function (see the next section below). The attenuation of the signal results from partial reflection of the signal by the impedance mismatch between the TEM sample holder and the pulse generator. The transformation of the signal results either from such reflections or from the rise and fall times of the signal generator.

5.2. Different pulse shapes

Given that continuous exposure electron holography is not limited to square pulses, we discuss here the possibility of using other pulse shapes. The theory for the use of different pulse shapes was presented in Section 3.4. Fig. 10 shows the dependence of the reconstructed amplitude on the shape of the wave applied between two metallic needles. The amplitude of each wave is 5 V and the frequency is 5 Hz. Although the amplitude of the excitation is the same, the positions of the equiphase contours (*i.e.*, amplitude minima) are different (see the line profiles in Fig. 10). For sine and triangle waves, the global maximum in the amplitude corresponds to zero phase difference and coincides with one of the metal electrodes, while points that are further from this region appear darker in the amplitude image. For dynamic experiments, the possibility of distinguishing different wave shapes can be used to detect a transformation of the signal in the specimen. Another advantage of using different wave shapes is the possibility to detect the region in the image where the phase difference between two states is zero.

5.3. Future experiments and instrumental requirements

This section discusses future experiments involving pulse modulation and resonance phenomena, as well as the possible use of more complicated pulse shapes to facilitate quasi-static switching experiments.

5.3.1. Dynamic experiments with pulse modulations

Consider a system that is able to switch reproducibly between two states. Assuming that the response time of the system to the excitation is limited, the response signal will depend on the frequency of a square wave input. Fig. 11 shows a schematic diagram of an excitation signal in the bottom graph and a possible system response at the top. If the frequency of the exciting square wave is increased, then a pronounced change in the shape of the response may occur (*i.e.*, sharp edges in the square pulse will become curved, as shown in the red dashed line in Fig. 11). As the reconstructed amplitude is sensitive to the pulse shape, the transition from square pulses to different pulse shapes can be detected. If one increases the excitation frequency further, so that the pulse duration is shorter than the system's time constant, then the system will not be able to switch between the two outermost states (as shown in the form of a solid blue line in Fig. 11), resulting in a decrease in the magnitude of the response signal in addition to its shape modulation. By performing frequency-dependent measurements, one can in principle therefore determine the time constant of the system.

5.3.2. Dynamic experiments under resonance conditions

A system that is triggered with a sine wave will show an amplified response under a resonance condition (during a frequency sweep), resulting in an increase in the magnitude of a signal recorded using continuous exposure electron holography. Resonances of electromagnetic fields, including damping effects, can therefore be studied with nm spatial resolution. For a given pulse frequency, the hardware requirements for experiments involving the use of sinusoidal pulse shapes are lower than those required for square pulse shapes.

5.3.3. Quasi-static experiments using combinations of pulses

Here, we propose a quasi-static magnetic switching experiment, which involves the use of combinations of square pulses to probe different parts of hysteresis and remanent hysteresis loops of nanoscale magnetic materials and devices. Fig. 12 (left panel) shows (*a*-c) possible pulse shapes that could be sent to a magnetising coil to access (a) the difference between states *B* and *D* in a hysteresis cycle (d); (b) the difference between two remanent states and (c) the difference between two saturated states *A* and *C*. In the first case (a), the first pulse denoted *A* is used to saturate the specimen magnetically in the positive direction (point *A* in the hysteresis cycle). A subsequent reduction in applied field to *B* provides access to point *B* in the hysteresis cycle. The reversed pulses *C* and *D* work in the opposite direction. Pulses *A* and *C* should be short in comparison to pulses *B* and *D*. A signal recorded using continuous exposure electron holography while sending such pulses will record the phase difference between states *B* and *D*. The frequency of the pulses and the precise pulse shape should be selected according to the magnetic response of the system.

6. Conclusions

Double and continuous exposure electron holography have been described theoretically and extended experimentally, in particular for studies of time-varying electrostatic potentials and magnetic fields. Following a brief comparison with conventional off-axis electron holography (Section 3.3), the theoretical description of double and continuous exposure electron holography was presented in Section 3. Approaches that can be used to remove the effects of absorption in the specimen and to unwrap reconstructed phase difference images have been proposed (Section 4.1) and the use of different pulse shapes to access time-resolved experiments has been discussed (Sections 5.2 and 5.3). It has been shown that the method can be used to perform frequency-dependent measurements of resonance phenomena and switching process with nm spatial resolution. The full application of the technique requires the development of dedicated high frequency TEM specimen holders that allow complicated pulse shapes to be used.

Note added during revision

It came to the authors' attention during revision of this manuscript following referees' comments that a similar paper had

Please cite this article as: V. Migunov, et al., Prospects for quantitative and time-resolved double and continuous exposure off-axis electron holography, Ultramicroscopy (2016), http://dx.doi.org/10.1016/j.ultramic.2016.08.010

been submitted by Gatel et al. at almost the same time as the present paper. Reference to the work of Gatel et al. was therefore included in the present manuscript during revision as Ref. [18].

Acknowledgements

We acknowledge Christophe Gatel and Etienne Snoeck from CEMES-CNRS in Toulouse for drawing our attention to the possibilities of high frequency double exposure off-axis electron holography. We are grateful to Michael Farle and AG Farle at the University of Duisburg-Essen for technical help, Enrico Nichelatti for valuable discussions and the European Union Seventh Framework Programme for funding under Grant Agreement 312483-ESTEEM2 (Integrated Infrastructure Initiative-I3). The research leading to these results has received funding from the European Research Council under the European Union's Seventh Framework Programme (FP7/2007-2013)/ ERC grant agreement number 320832.

References

[1] H. Wahl, Bildebenenholographie mit Elektronen, University of Tübingen, Habilitationsschrift, 1975.
[2] L.O. Heflinger, R.F. Wuerker, R.E. Brooks, Holographic interferometry, J. Appl. Phys. 37 (2) (1966) 642–649, http://dx.doi.org/10.1063/1.1708231.
[3] P. Hariharan, Optical Holography: Principles, Techniques and Applications, Cambridge University Press, Cambridge, 1996.
[4] H. Wahl, Experimentelle Ermittlung der komplexen Amplitudentransmission nach Betrag und Phase beliebiger elektronenmikroskopischer Objecte mittels der Off-Axis-Bildebenenholographie, Optik 28 (1968) 417–420.
[5] G. Matteucci, G.F. Missiroli, E. Nichelatti, A. Migliori, M. Vanzi, G. Pozzi, Electron holography of long range electric and magnetic fields, J. Appl. Phys. 69 (4) (1991) 1835–1842, http://dx.doi.org/10.1063/1.348970.
[6] G. Matteucci, G.F. Missiroli, M. Muccini, G. Pozzi, Electron holography in the study of the electrostatic fields: the case of charged microtips, Ultramicroscopy 45 (1) (1992) 77–83.
[7] S. Frabboni, G. Matteucci, G. Pozzi, Observation of electrostatic fields by electron holography: the case of reverse-biased p-n junctions, Ultramicroscopy 23 (1) (1987) 29–37.
[8] G. Matteucci, G.F. Missiroli, J.W. Chen, G. Pozzi, Mapping of microelectric and magnetic fields with double exposure electron holography, Appl. Phys. Lett. 52 (3) (1988) 176–178, http://dx.doi.org/10.1063/1.99511.
[9] G. Matteucci, G.F. Pozzi, Electron holography of long-range electrostatic, in: P. W. Hawkes (Ed.), Advances in Imaging and Electron Physics, 122, Elsevier, London, 2002, pp. 173–249.
[10] T. Hirayama, G. Lai, T. Tanji, N. Tanaka, A. Tonomura, Interference of three electron waves by two biprisms and its application to direct visualization of electromagnetic fields in small regions, J. Appl. Phys. 82 (2) (1997) 522–527, http://dx.doi.org/10.1063/1.365610.
[11] K. Harada, T. Akashi, Y. Togawa, T. Matsuda, A. Tonomura, Optical system for double-biprism electron holography, J. Electron Microsc. 54 (1) (2005) 19–27, http://dx.doi.org/10.1093/jmicro/dfh098.
[12] A. Ohshita, M. Okuhara, C. Matsuya, K. Hata, K. Iida, Direct visualization of electromagnetic microfields by superposition of two kinds of electron holograms, Microchim. Acta 155 (1–2) (2006) 225–228, http://dx.doi.org/10.1007/s00604-006-0547-4.
[13] J.J. Kim, D. Shindo, Y. Murakami, W. Xia, L.-J. Chou, Y.-L. Chueh, Direct observation of field emission in a single $TaSi_2$ nanowire, Nano Lett. 7 (8) (2007) 2243–2247.
[14] D. Shindo, J.J. Kim, W. Xia, K.H. Kim, N. Ohno, Y. Fujii, N. Terada, S. Ohno, Electron holography on dynamic motion of secondary electrons around sciatic nerve tissues, J. Electron Microsc. 56 (1) (2007) 1–5.
[15] M. Beleggia, G. Pozzi, Comment on 'Electron holography on dynamic motion of secondary electrons around sciatic nerve tissues', J. Electron Microsc. 57 (5) (2008) 165–167, http://dx.doi.org/10.1093/jmicro/dfn015.
[16] T. Matsuda, A. Fukuhara, T. Yoshida, S. Hasegawa, A. Tonomura, Q. Ru, Computer reconstruction from electron holograms and observation of fluxon dynamics, Phys. Rev. Lett. 66 (4) (1991) 457–460, http://dx.doi.org/10.1103/PhysRevLett.66.457.
[17] H. Ryll, M. Simson, M. Den Hertog, R. Dunin-Borkowski, K. El Hajraoui, R. Hartmann, M. Huth, S. Ihle, V. Migunov, J. Schmidt, H. Soltau, L. Strüder, Imaging at the timescale of micro- and milliseconds with the pnCCD (S)TEM camera, Microsc. Microanal. 21 (Suppl. S3) (2015) S1585–S1586, http://dx.doi.org/10.1017/S1431927615008703.
[18] C. Gatel, F. Houdellier, E. Snoeck, Dynamical holographic Moirés in a TEM, J. Phys. D: Appl. Phys. 49 (32) (2016) 324001, http://dx.doi.org/10.1088/0022–3727/49/32/324001.
[19] M.R. McCartney, D.J. Smith, Electron holography: phase Imaging with nanometer resolution, Annu. Rev. Mater. Res. 37 (2007) 729–767.
[20] V. Migunov, A. London, M. Farle, R.E. Dunin-Borkowski, Model-independent measurement of the charge density distribution along an Fe atom probe needle using off-axis electron holography without mean inner potential effects, J. Appl. Phys. 117 (13) (2015) 134301, http://dx.doi.org/10.1063/1.4916609.
[21] H. Lichte, M. Lehmann, Electron holography – basics and applications, Rep. Prog. Phys. 71 (1) (2008) 016102.
[22] R.A. McLeod, M. Bergen, M. Malac, Phase measurement error in summation of electron holography series, Ultramicroscopy 141 (2014) 38–50, http://dx.doi.org/10.1016/j.ultramic.2014.03.001.
[23] S.L.Y. Chang, C. Dwyer, J. Barthel, C.B. Boothroyd, R.E. Dunin-Borkowski, Performance of a direct detection camera for off-axis electron holography, Ultramicroscopy 161 (2016) 90–97, http://dx.doi.org/10.1016/j.ultramic.2015.09.004.
[24] F. Röder, A. Lubk, D. Wolf, T. Niermann, Noise estimation for off-axis electron holography, Ultramicroscopy 144 (2014) 32–42, http://dx.doi.org/10.1016/j.ultramic.2014.04.002.
[25] K. Ishizuka, Optimized sampling schemes for off-axis holography, Ultramicroscopy 52 (1) (1993) 1–5, http://dx.doi.org/10.1016/0304–3991(93)90017-R.
[26] F.F. Medina Estrada, G.F. Missiroli, E. Nichelatti, Amplificazione digitale di fase di ologrammi elettronici in doppia esposizione, in: XVIII Congresso di Microscopia Elettronica, Padova 24-28 Settembre, Suppl. di "Microscopia Elettronica" n.2, 1991, pp. 411–412.
[27] J.C. Mason, D.C. Handscomb, Chebyshev Polynomials, CRC Press, London, 2002.
[28] A. Tonomura, Electron Holography: Springer Series in Optical Sciences, 2nd ed., Springer, Berlin, 1999.
[29] C.J. Tay, C. Quan, F.J. Yang, X.Y. He, A new method for phase extraction from a single fringe pattern, Opt. Commun. 239 (4–6) (2004) 251–258, http://dx.doi.org/10.1016/j.optcom.2004.05.046.
[30] O.-H. Kwon, A.H. Zewail, 4d electron tomography, Science 328 (5986) (2010) 1668–1673, http://dx.doi.org/10.1126/science.1190470.

Please cite this article as: V. Migunov, et al., Prospects for quantitative and time-resolved double and continuous exposure off-axis electron holography, Ultramicroscopy (2016), http://dx.doi.org/10.1016/j.ultramic.2016.08.010